energies

MDPI

Article

Simulation of the Steam Gasification of Japanese Waste Wood in an Indirectly Heated Downdraft Reactor Using PRO/II™: Numerical Comparison of Stoichiometric and Kinetic Models

Gabriel Talero and Yasuki Kansha *

Organization for Programs on Environmental Sciences, Graduate School of Arts and Sciences, The University of Tokyo, 3-8-1 Komaba, Meguro-ku, Tokyo 153-8902, Japan; gftaleror@g.ecc.u-tokyo.ac.jp
* Correspondence: kansha@global.c.u-tokyo.ac.jp

Abstract: The conversion of biomass to olefin by employing gasification has recently gained the attention of the petrochemical sector, and syngas composition is a keystone during the evaluation of process design. Process simulation software is a preferred evaluation tool that employs stoichiometric and kinetic approaches. Despite the available literature, the estimation errors of these simulation methods have scarcely been contrasted. This study compares the errors of stoichiometric and kinetic models by simulating a downdraft steam gasifier in PRO/II. The quantitative examination identifies the model that best predicts the composition of products for the gasification of Japanese wood waste. The simulation adopts reaction mechanisms, flowsheet topology, reactions parameters, and component properties reported in the literature. The results of previous studies are used to validate the models in a comparison of the syngas composition and yield of products. The models are used to reproduce gasification at temperatures of 600∼900 °C and steam-to-biomass mass ratios of 0∼4. Both models reproduce experimental results more accurately for changes in the steam-to-biomass mass ratio than for temperature variations. The kinetic model is more accurate for predicting composition and yields, having global errors of 3.91%-mol/mol and 8.16%-g/g_{BM}, respectively, whereas the simple stoichiometric model has an error of 7.96%-mol/mol and 16.21%-g/g_{BM}.

Keywords: gasification; simulation; kinetic model; equilibrium model; error; biomass; waste wood; Japan; PRO/II

Citation: Talero, G.; Kansha, Y. Simulation of the Steam Gasification of Japanese Waste Wood in an Indirectly Heated Downdraft Reactor Using PRO/II™: Numerical Comparison of Stoichiometric and Kinetic Models. *Energies* **2022**, *15*, 4181. https://doi.org/10.3390/en15124181

Academic Editors: Petar Varbanov, Xuexiu Jia and Xue-Chao Wang

Received: 6 May 2022
Accepted: 2 June 2022
Published: 7 June 2022

1. Introduction

Biomass resources have been a controversial choice for energy utilization in the last decade because of possible negative effects relating to energy crop deforestation, food security, and biogenic CO_2 emissions [1]. The latest misuse of biomass can be traced to a highly dependent carbon-based economy. Additionally, Dente et al. [2] ascribed the negative effects of biomass use to the lack of a more effective bio-based circular economy and a clear valorization of biomass. It is crucial to consider biomass utilization for added-value purposes, such as the production of food, fertilizers, pharmaceuticals, and chemicals. The chemical sector faces several sustainability threats that can be addressed with rational biomass use [3]. In 2020, the industrial sector contributed 24% of global greenhouse gas emissions, and almost 5.8% of this contribution was from the petrochemical sector (including emissions from direct industrial processes and energy consumption) [4]. Yet the mitigation of CO_2 emissions in the energy sector has been tackled by shifting the carbon cycle economy, such as through the use of fuel cells and photovoltaic solar energy. This strategy cannot be directly applied to most carbon-based chemical subsectors. For instance, containers used for several everyday commodities (from food and pharmaceutical packing to disinfecting products used to limit the spread of COVID-19) are made according to sanitary and health standards, traditionally using organic chemicals such as polymers and resins [1].

In recent decades, biomass has been proposed as a renewable alternative to fossils in the petrochemical sector [3]. Life-cycle analysis has shown that the production of steam-cracking petrochemicals can be mitigated by producing bioplastics from biomass-derived ethylene, propylene, and BTX (i.e., a mixture of benzene, toluene, and xylenes) [5]. Light olefins (i.e., ethylene, propylene, and other C4 streams) are key petrochemical building blocks that are currently under revision for sustainability efforts, particularly in the selection of a suitable feedstock [6]. Within the spectrum of biomass sources, solid waste biomass is of great interest by not competing with food security or promoting deforestation [2]. Regardless of the low availability and expensive collection and management of waste biomass, this feedstock fits the agenda of a sustainable bio-based circular economy and waste management. The Japanese case study of bio-product utilization is of great interest, as Japan is the fourth largest consumer of petrochemicals and the fifth largest biomass market worldwide. Although its efficient waste management program maintained a biomass recycling ratio near 71% in 2020, most available lignified biowaste is forest wood waste (from leftover/thinning waste), rice residue (from straw/husk), and cardboard. Previous studies forecast a theoretical substitution of 21% of fossil-based petrochemicals (olefins and BTX) with biomass-based feedstock in Japan [7].

The conversion of biomass to olefins (BTO) remains at a conceptual level of design and many questions regarding chemical concepts and optimized pathways in a biorefinery remain unsolved [8]. For instance, there is no consensus on the use of direct BTO with catalytic reactions, and several studies have suggested the use of intermediate platforms such as methanol and dimethyl ethers [5]. Currently, most commercial-scale biorefineries are designed to yield methanol as a biofuel, commonly adopting the biochemical conversion of biomass possessing low lignin content [9]. The abundance of forest residue in Japan hinders traditional conversion through biochemical pathways, and lignified biowaste is, thus, converted alongside thermochemical pathways that easily decompose lignin [10]. In the framework of thermochemical conversion, gasification and synthesis gas (syngas) platforms play the main role in decomposing the complex lignocellulosic structures of biomass [11]. Steam gasification is a preferred technology that promotes clean syngas with high contents of H_2 and CO and is favorable for the synthesis of methanol and dimethyl ether [12]. Still, the evaluation of different BTO process scenarios requires calculations that rely on physical or numerical models at a conceptual level [13].

Accordingly, the numerical modeling of gasification is a fundamental approach for assessing different upstream conversion steps (e.g., direct syngas to olefins and additional platforms such as methanol) [14]. Gasification has been widely studied and modeled in recent decades owing to a high interest in the production of syngas for energy use [15]. Different simulation approaches include the use of dimensional and dimensionless models that solve a set of conservation equations (e.g., mass, momentum, energy, and species) with respect to space and time. Regarding space variations, dimensional models solve the conservation equations over a discrete region, while dimensionless models ignore gradients of properties within the reactor. A detailed mechanical design usually adopts dimensional models that include computational fluid dynamic models, while conceptual and plant designs mostly use dimensionless models. Temporal variations during gasification are included in the models by assuming an infinite (e.g., thermodynamic equilibrium approach) or fixed reaction time (e.g., kinetic approach). Equilibrium models neglect the geometry of the gasifier and assume an infinite reaction time to reach thermodynamic equilibrium. This assumption can be made by applying equilibrium constants (in the case of stoichiometric models) or by minimizing the Gibbs free energy (in the case of nonstoichiometric models). Non-stoichiometric models assume a stable equilibrium by solving the conservation equations at a minimum value of the Gibbs free energy of formation and restricting the mass balance of individual elements between reactants and products. Non-stoichiometric reactors are preferred, despite their lower precision, because a particular reaction mechanism is not required to predict the yield of products [16].

Unfortunately, the adoption of a thermodynamic equilibrium idealizes gasification to a maximum yield of products while excluding the residence time of the reactants, resulting in highly unrealistic results that overlook the geometric design. Meanwhile, kinetic modeling acknowledges reactant conversion rates by involving parameters such as residence time, temperature, and hydrodynamic parameters, enabling the simulation of complex reactors (e.g., fixed bed, fluidized bed, and entrained flow gasifiers) [17]. Still, the kinetic approach demands detailed information of the gasification mechanism, normally obtained experimentally or by making several assumptions [18]. In general, both equilibrium and kinetic approaches enable the simulation of gasification with material and energy integration, incurring a narrowing-down error. Mutlu et al. [15] comprehensively reviewed recent simulations conducted in Aspen Plus. They recommended implementing equilibrium models to establish a basic relationship between operating conditions and kinetic models for extensive process modeling.

The implementation of a BTO simulation demands the initial selection of one of the former modeling approaches. Most BTO studies have modeled gasification with a simple non-equilibrium approach (using Gibbs reactors or yield blocks) [8], rarely including an extensive validation of the gasification and reporting a simulation error below 5% [6]. Nonetheless, sensibility analyses of the reaction temperature or reactant content using simplified gasification models can be inaccurate [19]. Currently, there is no clear quantification of the simulation errors when selecting one model or another. For instance, Gonzalez et al. [20] compared the performances of stoichiometric and non-stoichiometric reactors in Aspen, concluding that the former reactor provides a better fit with experimental results. In this comparison, they excluded a detailed error quantification and only reported the global simulation errors of 2.1% v/v and 7.3% v/v for stoichiometric and non-stoichiometric reactors, respectively. Yu et al. [16] made a similar comparison between kinetic and non-stoichiometric reactors, concluding that the kinetic reactor provides a better fit with experimental data. They reported the relative error in the simulation only for the molar fractions of CO and CO_2, which ranged from 11% to 200%, excluding the error in the prediction of product yields.

The present paper compares the fitting of simulation results of stoichiometric and kinetic models with the parametric performance of a downdraft gasifier. This examination aims to identify the model that best predicts the composition of products during the gasification of Japanese wood waste and to quantify the lowest estimation error. The paper focuses on the mass balance of the steam gasification as a function of temperature (T) and the steam-to-biomass ratio (S/B). The models are implemented in PRO/II™, following the reaction mechanism for the gasification in a downdraft reactor [21]. The properties of components and the performance of the gasification are obtained from previous studies on Japanese wood waste [22]. Additionally, the previous studies contribute to the validation of the models in a comparison of the syngas composition and the yield of products [23]. The last section discusses the prediction error of each evaluated model and makes comparisons with results from the literature [24]. This study proposes a novel comparison of gasification with stoichiometric and kinetic approaches, using an alternative simulation software such as PRO/II™. This study also conducts an unusually extensive validation that enables a quantitative selection of a steam gasification model for further use in the biomass-to-petrochemical process design. As a result, this research precedes a more comprehensive study of the optimization of the thermochemical conversion of Japanese solid biowaste to biochemicals (light olefins), concerning the assessment of the environmental impact and techno-economic feasibility.

2. Gasification Mechanism

Gasification is a thermochemical conversion of organic compounds into synthesis gas (syngas) conducted from 600 to 1000 °C, using a reaction agent such as oxygen, steam, or CO_2. In the current study, biomass is considered an organic matter composed of carbon, hydrogen, and oxygen and free of inorganic matters and water for simplification. The

gasification of biomass (BM) encompasses a series of conversion substages that decompose, reduce, and rearrange the lignocellulosic structures of biomass into simpler molecules [15]. The initial stage of the former decomposition is called pyrolysis and occurs in absence of a reaction agent. In contrast to char gasification, where almost pure carbon is directly reduced with the reaction agent, biomass gasification requires pyrolysis to start reduction and rearrangement reactions [17]. Figure 1 summarizes the sequential decomposition of biomass into syngas through the operational units of drying, pyrolysis, gasification (reduction), and combustion. For modeling purposes, these substages are divided into separated zones regardless of the undefined boundaries in a real gasification operation.

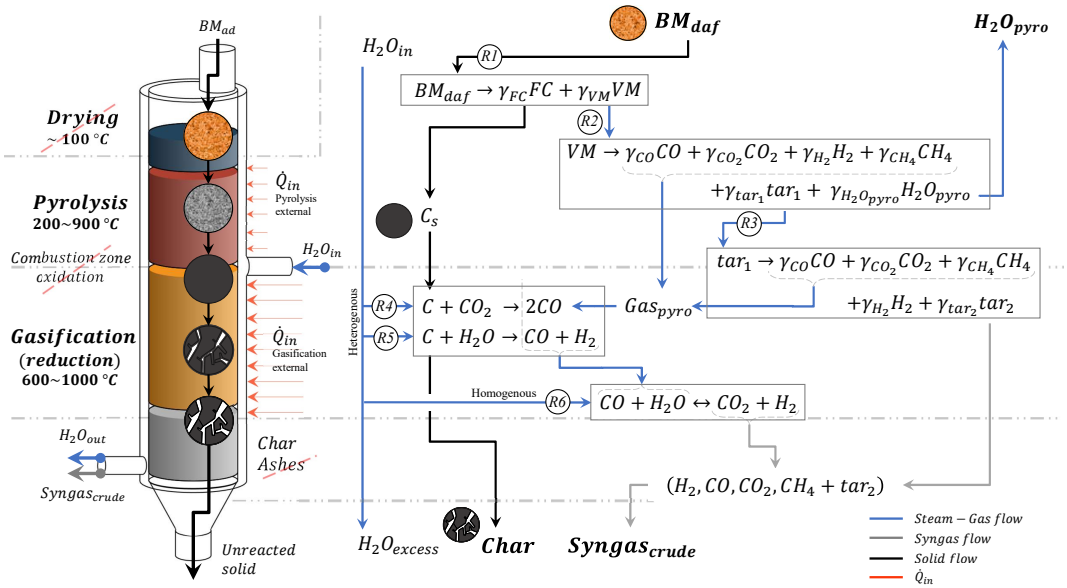

Figure 1. Flowchart of thermochemical conversions via gasification. **Left**: Mass and energy flow in a downdraft steam gasifier. **Right**: Reaction mechanism implemented in the current study.

The pyrolysis of biomass comprises a series of complex reactions (i.e., carbonization, devolatilization, and recondensation) in the absence of oxygen from 200 to 900 °C [25]. In the current study, pyrolysis is simplified in global reactions $R1$ and $R2$ (as shown in Figure 1), conducted at 500 °C [26]. The carbonization reaction performed during pyrolysis dramatically increases the carbon content in the solid phase, yielding solid carbon (C_s) with a yield near the fixed-carbon (FC) content present in the biomass. Meanwhile, the devolatilization reaction, $R2$, occurs near the volatile matter (VM) and produces several gases (i.e., CO, CO_2, H_2, and CH_4), primary tar (tar_1, defined as condensable organic compounds), and pyrolysis water H_2O_{pyro} [16]. Primary tar is reformed during the initial gasification stage to produce simple gases and secondary tar (tar_2), according to tar cracking reaction $R3$ [9].

During the operation of gasifiers such as downdraft, fluidized bed, and entrained flow gasifiers, pyrolysis products (i.e., carbon, pyrolysis gas, and tar) are collected and forced to stream to the combustion and reduction zones, reacting at a higher temperature [27]. Steam gasification is preferred over other reaction agents to maximize the content of H_2 in the syngas [17]. The presence of O_2 during gasification promotes the production of CO_2 in the combustion zone, leading to a high yield of CO and CO_2 in the reduction zone [28]. Recently, gasification involving supercritical water as a reaction agent (above the water critical point, 22.12 MPa and 374.12 °C) is proposed as an alternative concept for the conversion of wet biomass into syngas, since it reduces drying energy consumption and increases hydrogen yields [29]. Still, technical challenges remain unsolved for large-scale supercritical water gasification, such as the biomass feeding, salt precipitation, corrosion, or efficiency of heat exchangers. Consequently, large-scale steam gasifiers currently operate under subcritical conditions. Directly heated gasifiers supply the energy demand of the process through the

internal combustion of the pyrolysis products. In contrast, indirectly heated downdraft steam gasifiers have an external energy supply, and there is no combustion within the reactor (i.e., no oxygen is provided) [9]. The latter configuration hinders the production of CO_2 during gasification and increases the yield of H_2 [17].

The gasification zone includes heterogeneous and homogeneous reduction reactions at temperatures above 600 °C. The solid carbon reacts with the water stream and the pyrolysis gas in an adsorption/desorption heterogeneous mechanism analogous to a Langmuir–Hinshelwood mechanism, increasing the porosity of solid particles [30]. In the present study, heterogeneous reactions include only the Boudouard reaction, *R*4, and the water gas primary reaction, *R*5. The desorption gas, unreacted pyrolysis gas, and water steam undergo a homogenous water gas shift (WGS) reaction, *R*6. This paper excludes the methanation reaction because of the low content of CH_4 in steam gasification. Crude syngas comprises CO, CO_2, H_2, CH_4, and secondary tar. The unreacted char is usually burned in an external combustion reactor to generate the process's demanded heat or used as activated carbon for filtration systems [8].

3. Model Development and Methodology

The current study evaluated two gasification models, namely *StoicM* adopting a stoichiometric approach (i.e., using a thermodynamic equilibrium model) and *KinetM* adopting a kinetic approach. For both models, the process simulation followed the methodology for the material integration of an existing plant proposed by J. Haydary [13]. The operational units and gasification products were selected according to the mechanism discussed in Section 2. Section 3.2 presents the physical properties of the components whereas Section 3.3 presents the development of the flowsheet topology. The kinetic parameters of the two models are described in Sections 3.4 and 3.5. Finally, Section 3.6 reports the methodology for model validation.

AVEVA™ PRO/II™ Simulation 2020, as part of Schneider Electric SimSci, was used to simulate gasification and to predict the syngas composition and yield of products. PRO/II™ is a steady state and dynamic process simulator used in chemical process design and operational analysis. The functionality of PRO/II™ is similar to that of other commercial tools, such as Aspen Plus and Aspen HYSYS, deploying simulations via graphical user interfaces (GUI) and programming subroutines in Fortran [31]. Notwithstanding the versatility of PRO/II™ in chemical process engineering, gasification literature is scarce compared with the literature for AspenTech tools [32]. Therefore, the current methodology also adopted the simulation flowsheet reported by Mutlu et al. [15] for the modeling of biomass gasification in Aspen Plus.

3.1. Simulation Assumptions

Simplifications were made in the model development to fit the limitations of the simulation software [33], reduce the computational demand, and define unknown data [15]. The assumptions follow those reported in former studies [20]. For simplification, biomass is considered free of inorganic matter and initial water content. This approach limits the model to predict the catalytic effect of ash during gasification or the reactivity of the moisture content of biomass during the pyrolysis and gasification [30]. The following assumptions were applied for both *StoicM* and *KinetM*:

- The gasifier is a downdraft reactor with a capacity of 10 ton/h of woody biomass (daf) and a volume of 100 m^3, reproducing the design conditions of [34].
- The residence time is sufficient to reach steady-state conditions and the simulation blocks are zero-dimensional.
- Temperature gradients are neglected, emulating an isothermal process.
- The biomass is considered as dry and ash-free (daf), containing only carbon, hydrogen, and oxygen, while char contains only carbon. The catalytic effect of ash is ignored.
- Gases are assumed ideal. Pressure and heat losses are ignored.

- Tar is considered a homogeneous organic hydrocarbon containing only carbon, hydrogen, and oxygen.
- The reaction takes place in the absence of oxygen and no internal combustion or oxidation reactions take place.

3.2. Thermodynamic Method and Component Properties

The properties of components were estimated using the thermodynamic method of the Peng–Robinson cubic equation of state, coded in PRO/II™ as PR01. This method enables the calculation of properties for non-polar substances with phase changes. Conventional components included H_2O, CO, CO_2, H_2, CH_4, and *Char* (defined as pure carbon). The H_2O excludes the initial moisture content of biomass but corresponds to the steam used during the gasification (H_2O_{in}) and the water produced during pyrolysis (H_2O_{pyro}). Non-conventional compounds included biomass (BM), volatile matter (VM), fixed carbon (FC), and tar (tar). For simplification, the properties of tar were assigned to the components tar_1 and tar_2 in reaction $R3$. The thermochemical properties of the non-conventional components are presented in Table 1.

Table 1. Thermochemical properties of non-conventional components: biomass, char, and tar. N.A. means not applicable.

		BM				**Char**	**Tar**
Properties	**Unit**	**Wood Waste Average**	**Japanese Cedar [23,35]**	**Hinoki Cypress [36]**	**Japanese Red Pine [37]**	**Pure Carbon [38]**	**Bio-Oil [39]**
C_{daf}	% g/g	51.4 ± 2	50.4 ± 2.6	51.9 ± 0	51.9 ± 1.5	100	54.7 ± 9.8
H_{daf}	% g/g	6.2 ± 0.3	6.2 ± 0.2	6.2 ± 0	6.3 ± 0.4	0	6.6 ± 0.3
N_{daf}	% g/g	0.3 ± 0.3	0.7 ± 0.4	0.2 ± 0	0.1 ± 0.1	0	<0.9
O_{daf}	% g/g	42.2 ± 2.1	43.4 ± 2.6	41.8 ± 0	41.6 ± 1.6	0	38.7 ± 11.4
MC_{ad}	% g/g	21.8 ± 7.5	30.3 ± 12.3	27.7 ± 0	7.4 ± 2.7	0	52.1
VM_{daf}	% g/g	84 ± 4.1	83 ± 5	84.8 ± 0	84.2 ± 3.1	0	N.A.
FC_{daf}	% g/g	16 ± 4.1	17 ± 5	15.1 ± 0	15.8 ± 3.1	100	N.A.
HHV_{daf}	MJ/kg	21.1 ± 0.9	19.8 ± 1	23 ± 0	20.7 ± 0.8	39.35	37.3 ± 0.8
$\rho_{298K,daf}$ [40]	kg/m^3	405 ± 140	497	481	238	1611	1130
PRO/II™ properties of unconventional components—CxHyOz							
			BM	VM	FC	tar	
x	atom/atom-C		1	1	1	1	
y	atom/atom-C		1.49	1.79	0	1.43	
z	atom/atom-C		0.73	0.77	0	0.53	
MW	g/mol		23.83	26.24	12.01	21.98	
ΔH^0_{298K} [40]	MJ/kg		−10	−8	−30	−5.5	

The biomass used in the present study is Japanese waste wood. Former studies on Japanese waste management suggested a high availability of forestry residue (i.e., leftover treetops and branches) [7]. Forestry biomass quantification studies have concluded that Japanese cedar, Hinoki cypress, and Japanese red pine are the main tree species harvested [41]. For modeling purposes, the current study considered the properties of Japanese wood waste as an average across the above species. The properties of tar, including the ultimate composition, molecular weight (MW), enthalpy of formation (ΔH^0_{298K}), and density ($\rho_{298K,daf}$), were taken as constant values from Shrivastava et al. [39] and Popescu et al. [40]. The boiling point of tar was estimated as being at 180 °C and 1 atm for the manipulation of separation units [17].

3.3. Development of a Modeling Flow Diagram

Figure 2 presents the flowsheet topology of the gasification mechanism reported in Section 2 and shows the designs following similar studies from Chmielniak et al. [42] and Nikoo et al. [43]. Simulation nodes have rhombus shapes and represent the streams of the

components. BM_{daf} (node 1) is converted into FC (node 3) and VM (node 4) in the *decomposer* reactor at 500 °C and 101 kPa, according to reaction $R1$. The *decomposer* block is a conversion reactor (RConv) for both $StoicM$ and $KinetM$, considering a biomass conversion of 100%. FC is converted to the conventional component carbon. VM flows to a reactor called the pyrolyzer, where reaction $R2$ takes place at 500 °C and 101 kPa. Hereafter, the reactor blocks (i.e., the *pyrolizer*, *tar cracking* reactor, *heterogeneous gasifier*, and *homogeneous gasifier*) differ for each model, $StoicM$ and $KinetM$, according to Sections 3.4 and 3.5, respectively.

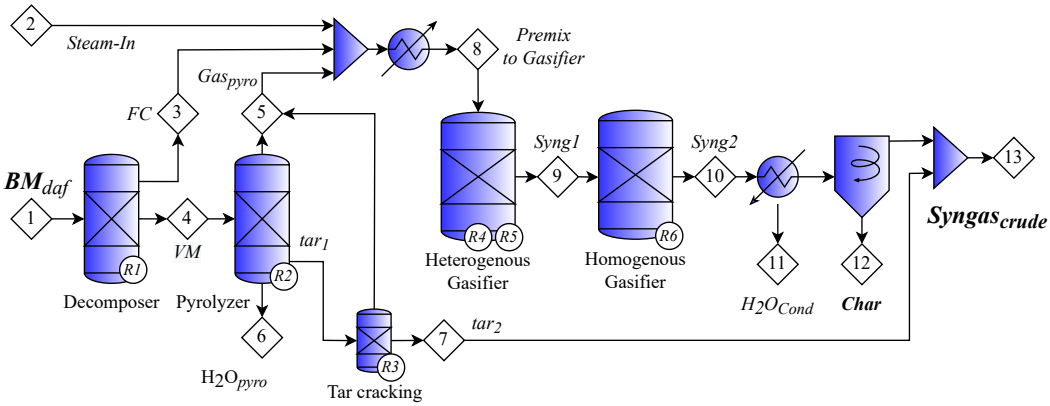

Figure 2. Flowsheet topology for the steam gasification of biomass in a downdraft reactor. The flow diagram definitions for models $StoicM$ and $KinetM$.

H_2O_{pyro} (node 6) flows out of the system, simulating the conditions of evaporation in the pyrolysis zone of a downdraft gasifier. tar_1 streams in the *pyrolizer* flow to the *tar cracking* reactor at 600 °C and 101 kPa, producing secondary tar (tar_2) [9]. The gas produced in the *pyrolizer* and *tar cracking* reactor is added to Gas_{pyro} (node 5). Gas_{pyro} and FC are mixed with the H_2O_{in} (node 2) or $Stream_{In}$ at 200 °C and 101 kPa. In the simulation, the steam-to-biomass mass ratio (S/B) ranges from 0 to 4 and is calculated with Equation (1). This premix to the gasifier ($Premix_{Gas}$ and node 8) is heated to gasification temperature (T) ranging from 600 to 900 °C.

$$S/B = \frac{\dot{m}_{H_2O_{in}}}{\dot{m}_{BMdaf}} \quad (1)$$

The gasification occurs at 101 kPa, and the reduction zone is divided into two reactor blocks called the *heterogeneous gasifier* and *homogeneous gasifier*. $Premix_{Gas}$ initially reacts according to the parallel heterogeneous reactions of Boudouard, $R4$, and water gas primary reaction, $R5$. The produced $Syng1$ (node 9), comprising the unreacted char and primary synthesis gases, flows to the *homogeneous gasifier* at constant temperature and pressure. This reactor converts $Syng1$ into the secondary synthesis gas $Syng2$ (node 10). The last section of the flowsheet comprises the separation of the unreacted steam H_2O_{cond} (node 11) at 0 °C and a cyclone that separates the solid (unreacted *char* and node 12) and gas phase $Syng_{dry}$. Finally, tar_2 and $Syng_{dry}$ are mixed to produce the crude syngas ($Syng_{crude}$ and node 13). $StoicM$ and $KinetM$ have the same simulation flow diagram (according to the following sections).

3.4. Stoichiometric Model StoicM

Table 2 presents the simulation conditions and defines the reaction parameters for the model $StoicM$. The layout of the simulation in PRO/II™ is detailed in Figure A1 of Appendix A. The *pyrolizer* block is a conversion reactor (RConv) with a 100% conversion of VM. The stoichiometric coefficients γ_i used for reaction $R2$ were calculated with Equation (2). The mass yield of each product (y_i) was taken from the product distribution of the pyrolysis of Japanese cedar at 500 °C [44]. Reactions $R1$ and $R2$ were performed in the same reactor, DECO + PYRO.

Table 2. Reaction conditions for model *StoicM*. The reaction parameters are taken from the literature; i.e., R1 and R2 are taken from [44], R3 from [40], R4 and R5 from [17], and R6 from [45]. T has a Kelvin unit.

Reactor Block (Rector Type)	Reaction		Reaction Parameters	Simulation Conditions
"DECO+PYRO" (RConv)	*R1*	$BM_{daf} \rightarrow \gamma_{FC}FC + \gamma_{VM}VM$	$\gamma_{FC} = 0.34$ $\gamma_{VM} = 0.75$	Fixed duty = 0 Conversion = 1
	R2	$\gamma_{VM}VM \rightarrow \gamma_{CO}CO + \gamma_{CO_2}CO_2 + \gamma_{H_2}H_2 + \gamma_{CH_4}CH_4 + \gamma_{tar_1}tar_1 + \gamma_{H_2O_{pyro}}H_2O_{pyro}$	$\gamma_{VM} = 0.75$, $\gamma_{CO} = 0.099$, $\gamma_{CO_2} = 0.077$, $\gamma_{H_2} = 0.08$, $\gamma_{CH_4} = 0.004$, $\gamma_{tar_1} = 0.3931$ $\gamma_{H_2O_{pyro}} = 0.26$	
"Tar cracking" (RConv)	*R3*	$tar_1 \rightarrow \gamma_{CO}CO + \gamma_{CO_2}CO_2 + \gamma_{CH_4}CH_4 + \gamma_{H_2}H_2 + \gamma_{tar_2}tar_2$	$\gamma_{CO} = 0.526$, $\gamma_{CO_2} = 0.0987$ $\gamma_{CH_4} = 0.18$, $\gamma_{tar_2} = 0.248$	Fixed duty = 0 Conversion = 0.72
"Heterogenous Gasifier" (REquil)	*R4*	$C + CO_2 \rightarrow 2CO$	$ln(K_P) = 21.335 - \frac{20743}{T}$	Fixed duty = 0 Activity basis = partial pressure
	R5	$C + H_2O \rightarrow CO + H_2$	$ln(K_P) = 17156 - \frac{16194}{T}$	
"Homogenous Gasifier" (REquil)	*R6*	$CO + H_2O \leftrightarrow CO_2 + H_2$	$ln(K_P) = 4.33 - \frac{4577.8}{T}$	Fixed duty = 0 Activity basis = partial pressure

The *tar cracking* block is a conversion reactor (RConv) assuming a 72% conversion of tar_1 [26]. Stoichiometric coefficients of $R3$ were taken for the tar lignin cracking [40]. The *heterogeneous gasifier* and *homogeneous gasifier* blocks are equilibrium reactors (REquil) fixed with an activity basis of partial pressure. The *heterogeneous gasifier* block takes equilibrium constants reported in the literature for both $R4$ and $R5$ (where T has Kelvin unit) [17]. Carbon is in solid phase and its activity exponent is zero. Finally, the *homogeneous gasifier* block takes equilibrium constants for $R6$ from [45].

$$\gamma_i = y_i \gamma_{VM} \frac{MW_{BM}}{MW_i} \tag{2}$$

3.5. Kinetic Model KinetM

Table 3 provides the simulation conditions and defines the reaction parameters for *KinetM*. The flowsheet of the simulation in PRO/II™ is detailed in Figure A2 of Appendix A. As in the *StoicK* model, the *decomposer* block is (RConv) considering a biomass conversion of 100%. For simulation purposes, the upstream reactors used in *KinetM* follow the PRO/II definition of the continuous-stirred-tank-reactor (CSTR) block.

The *pyrolizer* and *tar cracking* blocks used a kinetic definition of the pyrolysis for beechwood and tar reforming [26]. The *heterogeneous gasifier* and *homogeneous gasifier* blocks followed the kinetic formulation reported by Yu et al. [16]. Indeed, the reaction rates of $R4$ to $R6$ were defined with Equations (3) and (4) (E_a, r in units of kJ/mol and k_r in units of 1/s). Accordingly, the blocks were set with an activity basis of the molar concentration, and the activity exponent of carbon is zero.

$$r_{i,j} = k_r \prod_{i=1}^{N} [c_{i,j}]^{\alpha_{i,r}} \tag{3}$$

$$k_r = A_r T^{\beta} exp(-E_a/RT) \tag{4}$$

Table 3. Reaction conditions for the model *KinetM*. The reaction parameters are taken from the literature; i.e., R1 is taken from [44], R2 and R3 from [26], and R4 to R6 from [16]. T has a Kelvin unit.

Reactor Block (Rector Type)	Reaction		Reaction Parameters	Simulation Conditions
"Decomposer" (RConv)	*R1*	$BM_{daf} \rightarrow \gamma_{FC}FC + \gamma_{VM}VM$	$\gamma_{FC} = 0.34$ $\gamma_{VM} = 0.75$	Fixed duty = 0 Conversion = 1
"Pyrolyzer" (CSTR)	*R2*	$VM \rightarrow \gamma_{CO}CO + \gamma_{CO_2}CO_2 + \gamma_{H_2}H_2 + \gamma_{CH_4}CH_4 + \gamma_{tar_1}tar_1 + \gamma_{H_2O_{pyro}}H_2O_{pyro}$	$r_j = k_j \exp\left(-\frac{E_{a,j}}{RT}\right)(w_{VM}\rho_g)$ $k_{CO} = 9 \times 10^9$ / $E_{a,CO} = 110$ $k_{CO_2} = 5.23 \times 10^9$ / $E_{a,CO_2} = 105$ $k_{H_2} = 4.73 \times 10^4$ / $E_{a,H_2} = 92.5$ $k_{H_2O_{pyro}} = 3.6 \times 10^{13}$ / $E_{a,H_2O_{pyro}} = 150$ $k_{CH_4} = 1.09 \times 10^5$ / $E_{a,CH_4} = 71.3$ $k_{tar_1} = 2.09 \times 10^{10}$ / $E_{a,tar_1} = 112.7$	$\left\{ \begin{array}{c} k_j\ (1/s) \\ E_j\ (kJ/mol) \end{array} \right\}$ Fixed duty = 0 Reactor volume = 5 m^3
"Tar cracking" (CSTR)	*R3*	$tar_1 \rightarrow \gamma_{CO}CO + \gamma_{CO_2}CO_2 + \gamma_{CH_4}CH_4 + \gamma_{H_2}H_2 + \gamma_{tar_2}tar_2$	$r_{jcrack} = \gamma_j(10)^{4.98}\exp\left(\frac{-93.37}{RT}\right)(w_{tar_1}\rho_g)$ $\gamma_{CO} = 0.563$, $\gamma_{CO_2} = 0.111$ $\gamma_{H_2} = 0.017$, $\gamma_{CH_4} = 0.088$ $\gamma_{tar_2} = 0.2$	Fixed duty = 0 Reactor volume = 1 m^3
"Heterogenous Gasifier" (CSTR)	*R4* *R5*	$C + CO_2 \rightarrow 2CO$ $C + H_2O \rightarrow CO + H_2$	$A_rT^\beta = 589T$ / $E_a = 222.8$ $A_rT^\beta = 5.714T$ / $E_a = 129.7$	Fixed duty = 0 Reactor volume = 100 m^3
"Homogenous Gasifier" (CSTR)	*R6*	$CO + H_2O \leftrightarrow CO_2 + H_2$	$A_rT^\beta = 2.78$ / $E_a = 125.6$	Fixed duty = 0 Reactor volume = 1.5 m^3

This study acknowledges that a real gasifier is not completely represented by a CSTR reactor. Accordingly, efforts are made to emulate the gasification using CSTR blocks by adjusting simulation parameters. CSTR blocks are thus made to reflect the residence time of the components within the reactor by specifying a reactor volume. This residence time plays an important role in carbon conversion to syngas (X) [30]. For simulation purposes, the volume of the reactor was manually adjusted to fit the yield of products, the residence time, and X reported in the literature [16].

3.6. Methodology of Model Validation

The present paper uses experimental data reported in the literature for comparison and later model validation. Table 4 summarizes former studies that evaluated the steam gasification of Japanese woody biomass for different process parameters (i.e., T and S/B). Only Lit. 1 and Lit. 4 are used for the validation of the syngas composition and yield of products because they evaluate steam gasification under similar conditions, reporting complete in-service plant records (e.g., syngas composition, the yield of products, and statistic control). Indeed, Lit. 9 is a subsequent study of Lit. 1 and reports the scaling-up results for the steam gasification with Japanese woody biomass. The last approach increases the comparability of simulation results with experimental data, acknowledging the limitation of using different data sources of Lit. 1 and Lit. 4. Thus, the remaining complementary literature is used only for comparison purposes. Lit. 2 [46] is included to complement the data reported in Lit. 1 [18] for syngas composition during the steam

gasification in downdraft reactors. Likewise, Lit. 3 enhances the analysis of the effect of temperature on the syngas composition [22]. Unfortunately, these studies did not report product yields or carbon conversion. Hence, Lit. 4 [21] and Lit. 5 [47] were included to extend the revision to different gasifiers . Additionally, the inclusion of Lit. 6 allows analysis for a high steam content (i.e., S/B above 3) [23]. Lit. 1 to Lit. 6 were studies conducted on a laboratory scale, whereas Lit. 7 [35], Lit. 8 [24], and Lit. 9 [34] allow the comparison of gas composition in large-scale gasifiers.

Table 4. Results from the literature used in model comparison.

Source	Gasifier	Feedstock	Reaction Agent	T Range	S/B Range	Ref.
Lit. 1	Downdraft	Japanese cedar	Steam	500–900	0.6–3.2	[46]
Lit. 2	Downdraft	Red Pine	Steam	700–900	0.7–2.8	[18]
Lit. 3	Dual Fluidized	Wood pellets	Steam	770–850	0.75–1.6	[22]
Lit. 4	Fluidized bed	Waste wood	Steam	750–950	0.7	[21]
Lit. 5	Fixed bed	Waste wood	Steam	600–900	3.5	[47]
Lit. 6	Fixed bed	Japanese cedar	Steam	650–850	2.4–12	[23]
Lit. 7	Updraft	Japanese cedar	Steam	750	0.6–3.2	[35]
Lit. 8	Updraft	Japanese cedar	Air/Steam	850	0–1.4	[24]
Lit. 9	Updraft	Wood waste	Steam	950	2–4	[34]

For the model validation, this work adopts the definition of the systematic error (*Bias*) and total allowable error (*TEa*) proposed by Squara et al. [48]. *TEa* measures the simulation error by considering the dispersion of experimental data, because of the accuracy and calibration of equipment, or uncontrolled testing conditions [49]. The *Bias* is the absolute difference between a reference simulation value $y_{calc,i}$ and the mean value of the experimental results from the literature $y_{lit,i}$. TEa_i includes the coefficient of variation (CV_i) of the experimental results according to Equation (5). The root mean square (RMS) is used to quantify the accumulative difference (i.e., error) between models and experimental data of Lit. 1 [46] and Lit. 4 [21], according to Equation (6).

$$TEa_i = |y_{calc,i} - y_{lit,i}| + 1.65CV_i \tag{5}$$

$$RMS = \sqrt{\frac{\sum_{i=1}^{N}(TEa_i)^2}{N}} \tag{6}$$

The average CV_i for the syngas composition reported in Lit. 1 is 2.6%, 1.26%, 8.27%, and 8% for H_2, CO, CO_2, and CH_4, respectively [46]. In addition to the molar composition of the syngas, this study used X and $y_{products}$ to compare the simulation results with the experimental results reported in the literature on a dry and ash-free basis and according to Equations (7) and (8). The average CV_i for the yield of products reported in Lit. 4 is 9.09%, 3.32%, and 6.21% for X, y_{gas}, and y_{tar}, respectively [22]. Lit. 2, Lit. 3, and Lit. 5 do not report the standard deviation of experimental data.

$$y_{product,i} = \frac{\dot{m}_i}{\dot{m}_{BM_{daf}}} \times 100 \tag{7}$$

$$X = \frac{\dot{m}_{BM_{daf}} FC_{daf} - \dot{m}_{Char}}{\dot{m}_{BM_{daf}} FC_{daf}} \times 100 \tag{8}$$

4. Results and Discussion

4.1. Material Balance and Composition

Tables 5 and 6 give the material balance and composition of a baseline simulation for the models *StoicM* and *KinetM*, respectively. The baseline conditions are $T = 850$ °C and $S/B = 0.7$. The nodes used in the material balance correspond to the topology presented in

Figure 2. Mass flows ($\dot{m}_i$) are presented for the case study of a gasifier having a biomass (daf) consumption of 10 ton/h.

Table 5. Material balance and composition for the model *StoicM* at a temperature of 850 °C and S/B of 0.7. * The molar composition of VM corresponds to the products of the pyrolysis reaction after $R2$.

					Molar Composition						
Node	**Stream Unit**	$\dot{m}$ **ton/h**	T **°C**	**Pressure kPa**	**C**	**Tar**	**H_2O**	**H_2**	**CO**	**CO_2**	**CH_4**
					mol/mol						
Steams In											
1	BM	10.0	30	101							
2	$SteamIn$	7.0	200	101			1.0				
Pyrolysis											
3	FC	1.70	500	101	1.0						
4	VM *	8.30	500	101		0.429	0.287	0.087	0.108	0.085	0.004
5	Gas_{pyro}	5.30	0	101			0.003	0.164	0.507	0.215	0.112
6	H_2O_{pyro}	1.98	0	101			1.0				
7	tar_2	1.026	0	101		1.0					
Gasification											
8	$Premix_{Gas}$	13.81	850	101	0.195		0.522	0.046	0.144	0.061	0.032
9	$Syng1$	13.81	850	101	0.026		0.250	0.318	0.211	0.163	0.032
10	$Syng2$	13.81	850	101	0.026		0.324	0.245	0.285	0.089	0.032
11	H_2O_{cond}	4.20	0	101			1.0				
12	$Char$	0.224	0	101	1.0						
13	$Syngas_{crude}$	10.41	0	101		0.089	0.003	0.341	0.398	0.125	0.044

Table 6. Material balance and composition for the model *KinetM* at a temperature of 850 °C and S/B of 0.7. * The molar composition of VM corresponds to the products of the pyrolysis reaction after $R2$.

					Molar Composition						
Node	**Stream Unit**	$\dot{m}$ **ton/h**	T **°C**	**Pressure kPa**	**C**	**Tar**	**H_2O**	**H_2**	**CO**	**CO_2**	**CH_4**
					mol/mol						
Steams In											
1	BM	10.0	30	101							
2	$SteamIn$	7.0	200	101			1.0				
Pyrolysis											
3	FC	1.70	500	101	1.0						
4	VM *	8.30	500	101		0.544	0.178		0.247	0.026	0.005
5	Gas_{pyro}	6.53	0	101			0.001	0.231	0.603	0.033	0.132
6	H_2O_{pyro}	1.14	0	101			1.0				
7	tar_2	0.632	0	101		1.0					
Gasification											
8	$Premix_{Gas}$	15.04	850	101	0.170		0.455	0.087	0.226	0.012	0.050
9	$Syng1$	15.04	850	101	0.031		0.315	0.226	0.366	0.012	0.050
10	$Syng2$	15.04	850	101	0.031		0.211	0.330	0.262	0.116	0.050
11	H_2O_{cond}	3.13	0	101			1.0				
12	$Char$	0.304	0	101	1.0						
13	$Syngas_{crude}$	12.23	0	101		0.044	0.003	0.415	0.330	0.146	0.063

Pyrolysis converts 11% to 19% of the initial mass of biomass into H_2O_{pyro}, whereas 17% of the initial mass is converted into carbon for both models. After pyrolysis and tar cracking, 53% to 65% of the biomass mass is converted into Gas_{pyro} and almost 10% is converted into secondary tar. According to *KinetM*, approximately 85% of the primary tar is converted into tar_2 during tar cracking. This value is higher than the assumed conversion of 75% in *StoicM*. Consequently, *StoicM* predicts a lower $\dot{m}_{gas}$ than does *KinetM*, because the stoichiometric coefficients of $R2$ and $R3$ promote a higher production of H_2O_{pyro} and tar_2 with the model *StoicM*. Gas_{pyro} presents a molar content of H_2, CO, and CO_2 above

86%. Compared with *StoicM*, the kinetic model predicts a lower content of CO_2 in Gas_{pyro}, because of the lower value of γ_{CO_2} used in the kinetic tar cracking model (presented in Table 3).

The pyrolysis product distribution is similar to that reported in the literature [44]. The errors in the distribution of pyrolysis products predicted with *KinetM* and *StoicM* are, respectively, 7.2% and 6.4% [50]. The highest error is observed for *FC* owing to the assumption of the complete conversion of the solid phase into pure carbon. As a consequence of the product distribution after pyrolysis and tar cracking, *StoicM* produces almost 12% less Gas_{pyro} than does *KinetM*. This flow difference in the reactants results in lower reactivity during the gasification with *StoicM*, as evidenced by a higher unreacted $\dot{m}_{H_2O_{cond}}$ for this model. Indeed, *StoicM* seems to be more affected by the concentration of the reactants, in agreement with Le Chatelier's principle and the formulation of an equilibrium model [20].

While pyrolysis and tar cracking produce almost 53% g/g_{BM} of $Syngas_{crude}$, the remaining 47% g/g_{BM} reacts in the gasification zone, as a result of the reaction of *Char* and Gas_{pyro} in *R*4 to *R*6. Almost 3% of the initial biomass remains as unreacted carbon after the *heterogeneous gasifier*. The differences in $\dot{m}_{char}$ between *StoicM* and *KinetM* reveal a higher char conversation *X* in the former model. Indeed, the remaining char in *Stoic* is 13% g/g whereas that in *KinetM* is 18% g/g. The former variation is due to the equilibrium conditions of *R*4 and *R*5 in the stoichiometric model, where the char residence time in the reactor is ignored, and char conversion is overestimated [15]. In contrast, the reactor volume regulates the reaction rate in *KinetM*, providing a more realistic approach, with similar data reported in the literature [12].

The *heterogeneous gasifier*, as the final reactor, exposes different behaviors between models under the baseline conditions. In *KinetM*, the WGS reaction reduces the molar content of CO while increasing the contents of H_2 and CO_2. In contrast, *StoicM* adopts the reverse definition of the WGS reaction under baseline conditions, suggesting an equilibrium that reduces the contents of H_2 and CO_2. According to Sharma et al. [27], a rise in temperature above 770 °C reduces the hydrogen yield, in agreement with Le Chatelier's principle for the exothermic reaction *R*6. The effects of *T* and *S*/*B* on the syngas composition and the equilibrium conditions are discussed in the following sections to clarify the role of the reduction zone.

4.2. Model Validations

The models are validated by presenting the effects of *T* and *S*/*B* on the distribution of the products. The effect of *S*/*B* is assessed in the range from 0 to 4 with steps of 0.35 for a constant *T* of 850 °C. The effect of *T* is assessed in the range from 600 to 900 °C with steps of 50 °C for a constant *S*/*B* of 0.7. The prediction error of each model is presented as *RMS* for each gasification parameter (*T* and *S*/*B*) relative to results from the literature.

4.2.1. Effect of the Steam-to-Biomass Ratio (*S*/*B*)

Figure 3 presents the effect of *S*/*B* on the syngas composition at $T = 850$ °C, comparing *KinetM* and *StoicM*. The gas composition is reported on a dry basis (free of tar and water). Lit. 1 and Lit. 2 results are taken from [18,46], respectively.

The composition of the syngas at $S/B = 0$ illustrates the effect of pyrolysis and *tar cracking* blocks, specifically low char conversion below 10%. In this state of gasification, CO has the highest molar content among the constituents in the syngas for both models. A rise in the steam flow promotes the production of H_2 and CO_2 while reducing the contents of CO and CH_4. The profile trends are similar for *StoicM* and *KinetM* but with a sharp asymptotic behavior occurring for *KinetM*. This rapid change in the molar composition at *S*/*B* below 2 for *KinetM* is attributed to the concentration dependency of $r_{i,j}$ (Equation (3)) and not the partial pressure of *StoicM* (Table 2) [17]. In Figure 3, both models reproduce the trends of experimental results reported by Umeki et al.[46], and Huang et al. [18]. *KinetM* makes a better prediction of CO and H_2 contents whereas *StoicM* better reproduces variations in

CO_2 and CH_4 contents. Both models overestimate the molar fraction of CO_2 relative to results obtained by [20] (for an equilibrium reactor) and [16] (for Gibbs and CSRT reactors).

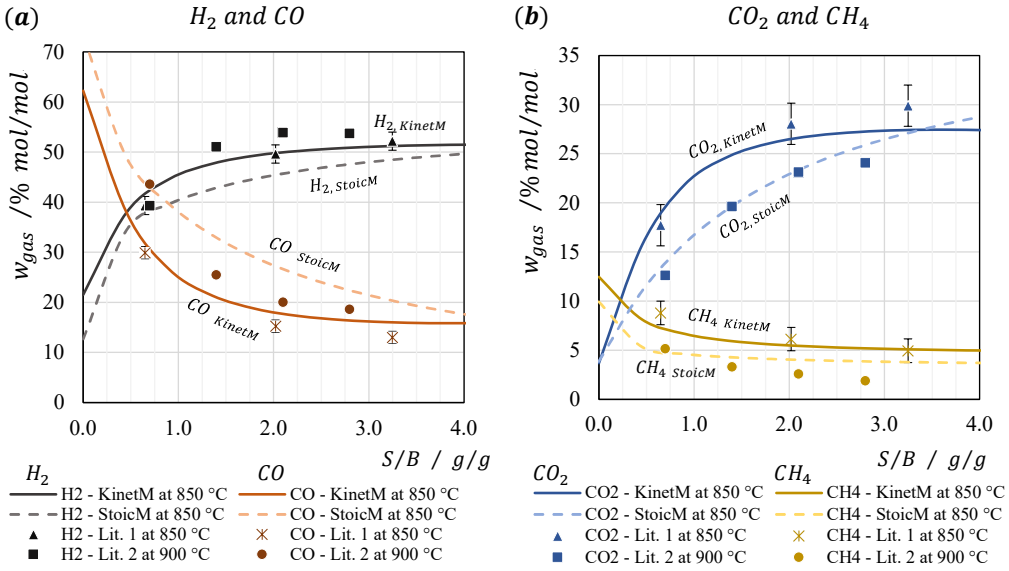

Figure 3. Effect of S/B on the dry syngas composition at $T = 800$ °C, comparing the results of *KinetM* (continuous lines) and *StoicM* (dashed lines) with results from the literature: (**a**) H_2 and CO. (**b**) CO_2 and CH_4. Lit. 1 and Lit. 2 results are taken from [18,46], respectively.

4.2.2. Effect of the Gasification Temperature (T)

Figure 4 presents the effect of T on the syngas composition (free of tar and water) at $S/B = 0.7$, comparing *KinetM* and *StoicM*. Raising T increases the yield of H_2 whereas it reduces the contents of CO and CH_4. The latter behavior is attributed to the greater conversion of char, boosting the roles of the heterogeneous reactions *R*4 and *R*5 [15]. Indeed, the water gas primary reaction (*R*5) increases the production of H_2 while consuming CO_2 and competing with the WGS reaction *R*6 [12]. Consequently, variations in the molar content of CO_2 do not follow clear trends in either the modeling or experimental results. The higher content of H_2 and the reduced content of CO after 700 °C suggest a leading role of *R*4 over the WGS and Boudouard reactions. Excluding CO_2, the profile trends are similar for *StoicM* and *KinetM*.

In contrast to the effect of S/B, there is no asymptotic behavior within the temperature range simulated. Additionally, the numerical difference between the results of *StoicM* and *KinetM* is notably higher when predicting w_{CO} and w_{CO_2} in the lower range of T. The latter disparity suggests differences in the reactivity of the char assumed in the models. Both models overpredict the molar content of H_2 and CO reported in the literature. Furthermore, Gonzalez et al. [20] reported a similar overestimation with equilibrium models related to differences in the experimental formation of secondary tar. A more extensive revision of tar reforming and cracking is advised in future simulation studies.

The char conversion affects the discrepancies between the literature and models. Figure 5 presents the effect of T on X and the yields of products (y_{gas} and y_{tar}) at $S/B = 0.7$, comparing *KinetM* and *StoicM*. There is a notable difference between the experimental and simulation char conversions at temperatures near 800 °C. Nevertheless, a better fitting of X was observed at 600 and 900 °C. Compared with the simulation results, a lower X in the experimental data suggests the lower production of CO and H_2 during gasification at 800 °C. Variations in X explain the better prediction of the syngas composition at higher temperatures. Furthermore, the former difference in X explains the inaccuracy of *StoicM* in predicting w_{CO} and w_{CO_2} in the lower T range.

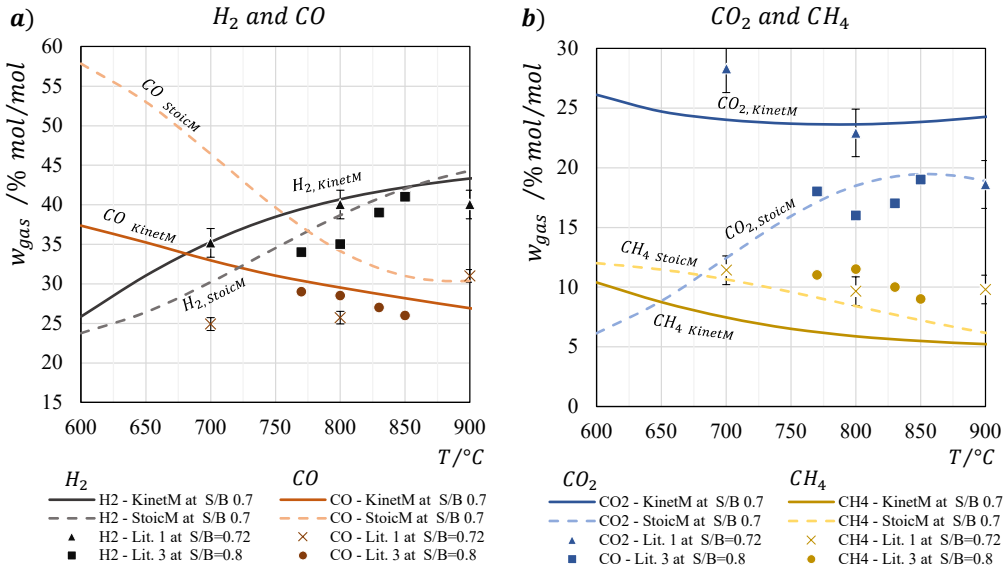

Figure 4. Effect of T on the dry syngas at $S/B = 0.7$, comparing *KinetM* (continuous lines) and *StoicM* (dashed lines) with results of the literature: (**a**) H_2 and CO. (**b**) CO_2 and CH_4. Lit. 1 and Lit. 3 are taken, respectively, from [22,46].

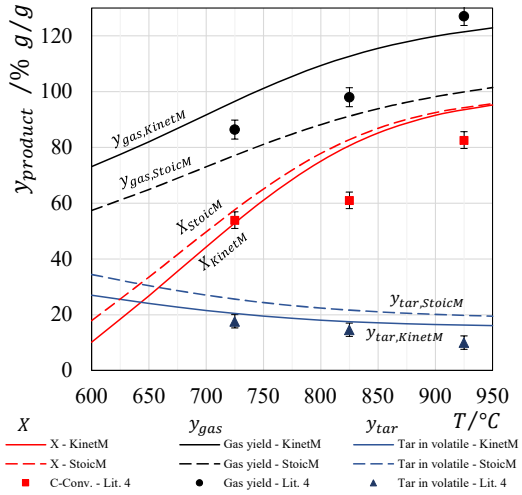

Figure 5. Effects of T on X, y_{gas}, and y_{tar}, comparing *KinetM* (continuous lines) and *StoicM* (dashed lines) with results of the literature. Lit. 4 is taken from [21].

The estimation of y_{gas} made using *KinetM* is higher than that made using *StoicM*. This discrepancy is explained by a higher production of gas during pyrolysis and tar cracking (as reported in Tables 5 and 6). The stoichiometric model seems to better predict y_{gas} at lower temperatures, but the fitting with experimental results is enhanced at temperatures near 900 °C. The results of y_{tar} obtained using the two models are similar and follow the literature data. The following section discusses the global performance of the models in detail, quantifying the discrepancies with the literature data and suggesting general trends in the fitting errors.

4.2.3. *RMS* Prediction Error of the Models

Table 7 presents the errors of models *StoicM* and *KinetM* in the prediction of the syngas composition ($w_{gas,i}$) and mass yield of the products ($y_{product,i}$) when evaluating T and S/B. *KinetM* has lower global error (RMS_{global}) than *StoicM* under all evaluation conditions. Both models are more accurate in predicting the effect of S/B than in predicting the effect of T. Indeed, the evaluation of S/B using *KinetM* has the best global fitting with

the experimental data of $w_{gas,i}$. In contrast, the prediction of the effect of T on $w_{gas,i}$ has a higher error using *StoicM*, mainly because of the overestimation of CO content. The error in the prediction of $y_{product,i}$ is higher than that in the prediction of $w_{gas,i}$, as the stoichiometric approach has a global *RMS* error exceeding 12%.

Table 7. The errors *RMS* of models *StoicM* and *KinetM* in the prediction of the syngas composition ($w_{gas,i}$) and mass yield of the products ($y_{product,i}$) when evaluating T and S/B.

	Error vs. T						**Error vs. S/B**	
	$RMS - w_{gas}$			$RMS - y_{product}$			$RMS - w_{gas}$	
Unit	***KinetM*** **% mol/mol**	***StoicM***		***KinetM*** **% g/g**	***StoicM***		***KinetM*** **% mol/mol**	***StoicM***
H_2	1.28	2.91	X	9.34	14.85	H_2	1.53	3.14
CO	5.24	13.88	Y_{gas}	9.66	22.14	CO	2.47	9.77
CO_2	4.01	5.49	Y_{tar}	4.38	8.79	CO_2	4.72	1.52
CH_4	3.05	1.22				CH_4	2.48	2.88
RMS_{global}	3.91	7.96		8.16	16.21		2.91	5.62

RMS_{global} reported in the literature for predicting $w_{gas,i}$ ranges from 2.1% to 14% mol/mol when using stoichiometric models [16] whereas RMS_{global} for kinetic models ranges from 1.3% to 4.4% mol/mol [16]. As an additional comparison, RMS_{global} reported in the literature for non-stoichiometric models (using Gibbs reactors) ranges from 5.15% to 11% mol/mol, similarly to the error range for stoichiometric models [51]. The simulation error is the largest for CO_2 among the constituents, but this error has not been discussed extensively. As presented in Section 4.1 and reported by Gonzalez et al. [20], the models are sensitive to overestimations of char conversion and tar cracking and reforming. These limitations suggest that kinetic models that include Langmuir–Hinshelwood mechanisms should be implemented.

5. Conclusions

The simulation of the downdraft gasifier with Japanese wood waste in PRO/II™ allowed the prediction of the syngas molar composition ($w_{gas,i}$) and the yield of products ($y_{product,i}$) with *RMS* errors below 7.96% mol/mol$_{gas}$ and 16.21% g/g$_{BM}$, respectively. A comparison between the fitting of kinetic and stoichiometric models to experimental data confirmed a higher accuracy when using the former model. Indeed, the adoption of a simpler stoichiometric model reduced the accuracy of the prediction of $w_{gas,i}$ and $y_{product,i}$, increasing the *RMS* error by 4.05% mol/mol and 8.05% g/g$_{BM}$, respectively. Both models better reproduced experimental results for changes in the steam-to-biomass ratio than for temperature variations. The error of the evaluated models is ascribed to an overestimation of char conversion in heterogeneous reactions, as well as the excessive production of pyrolysis gas previous to the gasification zone.

The results of the present study support recommendations made in the literature to use equilibrium models for basic relationships between operating conditions and kinetic models for more precise modeling evaluations. The current study makes an additional contribution by measuring and suggesting the simulation error when using Kinetic or Stoichiometric models Still, this paper acknowledges the limitations of the error definition and the narrow comparison of a single gasification case of study. Consequently, a further revision of different gasification scenarios is advised. Such a revision should include extended model validation with systematic reviews, contrasting non-equilibrium and dimensional models, and the evaluation of different biomass sources and reaction mechanisms.

Author Contributions: Conceptualization, G.T. and Y.K.; methodology, G.T.; software, G.T.; validation, G.T. and Y.K.; formal analysis, Y.K.; data curation, G.T.; writing—original draft preparation, G.T.; writing—review and editing, G.T. and Y.K.; visualization, G.T.; supervision, Y.K.; project administration, Y.K. All authors have read and agreed to the published version of the manuscript.

Funding: This research received no external funding.

Institutional Review Board Statement: Not applicable.

Informed Consent Statement: Not applicable.

Data Availability Statement: Data is contained within the article.

Conflicts of Interest: The authors declare no conflict of interest.

Abbreviations

The following nomenclature is used in this manuscript:

$\alpha_{i,r}$	Activity exponent of reaction r for component i in Equation (3) (mol);
ad	As determined basis;
γ	Stoichiometric coefficient (mol);
$\rho_{298K,daf}$	Density at a reference temperature of 298 K, 1 atm (kg/m^3);
$A_r T^{\beta}$	Constant for kinetic parameters in Equation (4)
BM	Biomass stream (mol/m^3);
$c_{i,j}$	Concentration (mol/m^3);
C_s	Carbon in solid state;
daf	Dry and ash-free basis;
db	Dry basis;
E_a	Energy of activation in Equation (4) (kJ/mol);
FC	Fixed carbon stream;
HHV_{daf}	High heating value (MJ/kg);
H_2O_{pyro}	Pyrolysis water stream;
ΔH^0_{298K}	Enthalpy of formation at 298 K (MJ/kg);
k_r	Pre-exponential coefficient (1/s);
K_P	Equilibrium constant;
$\dot{m}$	Mass flow (ton/h);
MC_{ad}	Moisture content (g/g$_{BM}$);
MW	Molecular weight (g/mol);
R	Gas constant = 8.314 J/Kmol;
$r_{i,j}$	Reaction rate (mol/s);
$R1$–$R6$	Reactions;
RMS	Relative mean square error (%);
S/B	Steam-to-biomass mass ratio (g/g$_{BM}$);
$StoicM$	Stoichiometric model;
tar	Volatile matter stream;
VM	Volatile matter stream;
w	Molar fraction (mol/mol);
X	Carbon conversion in gasification (g/g);
y	Mass yield or fraction (g/g$_{BM}$).

Appendix A

This appendix presents the layout of the simulation flowsheet in PRO/II, detailed in Figure A1 for model *StoicM* and Figure A2 for *KinetK*. The version of the software is *AVEVA™ PRO/II™ Simulation 2020*. The intermediate reactor CONV-PSEUDOS is used to convert the non-conventional component *FC* into the conventional component CARBON.

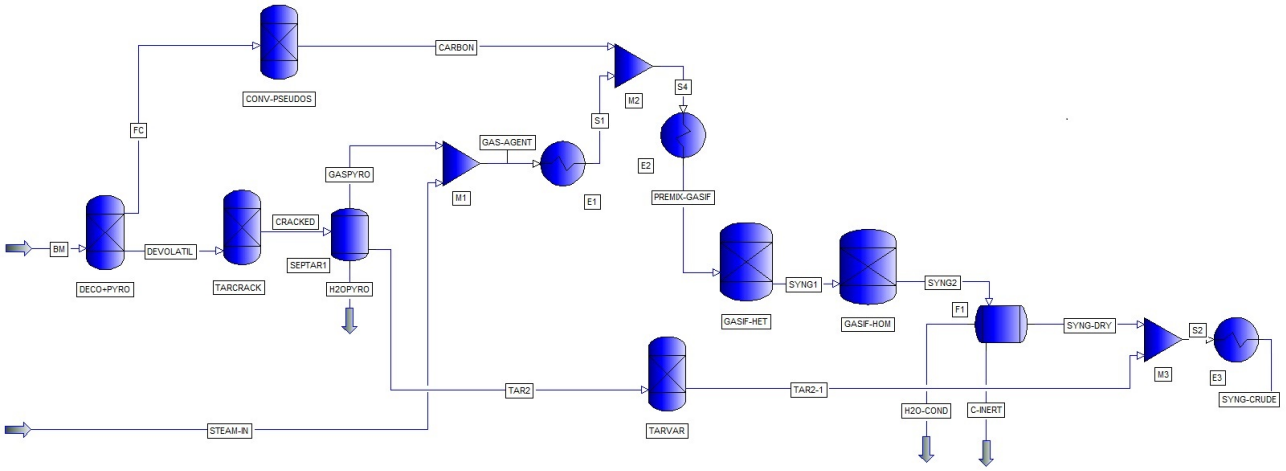

Figure A1. Flow diagram for the *StoicM* model in PRO/II.

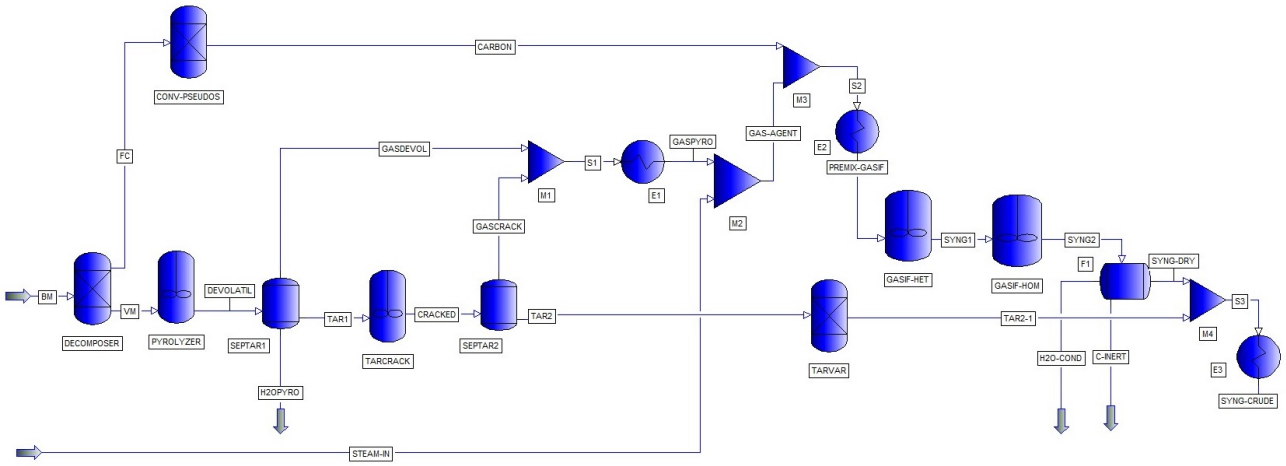

Figure A2. Flow diagram for the *KinetM* model in PRO/II.

References

1. Yadav, V.G.; Yadav, G.D.; Patankar, S.C. The production of fuels and chemicals in the new world: Critical analysis of the choice between crude oil and biomass vis-à-vis sustainability and the environment. *Clean Technol. Environ. Policy* **2020**, *22*, 1757–1774. [CrossRef]
2. Dente, M.R.; Kayo, C.; Aoki-suzuki, C.; Tanaka, D. Life cycle environmental impact assessment of biomass materials in Japan. *J. Clean. Prod.* **2020**, *257*, 120388. [CrossRef]
3. Hongo, T. Circular Economy Potential and Public-Private Partnership Models in Japan. In *Towards a Circular Economy: Corporate Management and Policy Pathways*; ERIA Research Project Report; Economic Research Institute for ASEAN and East Asia (ERIA): Jakarta, Indonesia, 2016; pp. 17–29.
4. IEA—International Energy Agency. *Global Energy Review: CO2 Emissions in 2021 Global Emissions Rebound Sharply to Highest Ever Level*; Technical Report; IEA—International Energy Agency: Paris, France, 2022.
5. Ren, X.Y.; Feng, X.B.; Cao, J.P.; Tang, W.; Wang, Z.H.; Yang, Z.; Zhao, J.P.; Zhang, L.Y.; Wang, Y.J.; Zhao, X.Y. Catalytic Conversion of Coal and Biomass Volatiles: A Review. *Energy Fuels* **2020**, *34*, 10307–10363. [CrossRef]
6. Arvidsson, M.; Haro, P.; Morandin, M.; Harvey, S. Comparative thermodynamic analysis of biomass gasification-based light olefin production using methanol or DME as the platform chemical. *Chem. Eng. Res. Des.* **2016**, *115*, 182–194. [CrossRef]
7. Talero, G.; Nielsen, C.M.; Kansha, Y. Identification of Japanese Solid Biowaste for Conversion into Biochemicals and Energy via Thermochemical Biorefinery. *Chem. Eng. Trans.* **2021**, *88*, 313–318. [CrossRef]
8. Jiang, P.; Parvez, A.M.; Meng, Y.; Xu, M.x.; Shui, T.c.; Sun, C.g.; Wu, T. Exergetic, economic and carbon emission studies of bio-olefin production via indirect steam gasification process. *Energy* **2019**, *187*, 115933. [CrossRef]
9. Herdem, M.S. Performance investigation of a non-combustion heat carrier biomass gasifier for various reforming methods of pyrolysis products. *Int. J. Green Energy* **2022**, *19*, 62–71. [CrossRef]
10. Kartal, F.; Özveren, U. A comparative study for biomass gasification in bubbling bed gasifier using Aspen HYSYS. *Bioresour. Technol. Rep.* **2021**, *13*, 100615. [CrossRef]

11. Talero, G.; Rincón, S.; Gómez, A. Biomass torrefaction in a standard retort: A study on oil palm solid residues. *Fuel* **2019**, *244*, 366–378. [CrossRef]
12. Zhao, S.; Ding, L.; Ruan, Y.; Bai, B.; Qiu, Z.; Li, Z. Experimental and kinetic studies on steam gasification of a biomass char. *Energies* **2021**, *14*, 7229. [CrossRef]
13. Haydary, J. *Chemical Process Design and Aspen Plus and Aspen HYSYS Applications*; John Wiley and Sons, Inc.: New Delhi, India, 2019.
14. Kansha, Y.; Ishizuka, M.; Tsutsumi, A.; Kambe, Y.; Yoshihara, J. Simulated Application of Self-Heat Recuperation and Pressure Swing System to Industrial Methanol Synthesis Process. *J. Chem. Eng. Jpn.* **2019**, *52*, 650–655. [CrossRef]
15. Mutlu, O.C.; Zeng, T. Challenges and Opportunities of Modeling Biomass Gasification in Aspen Plus: A Review. *Chem. Eng. Technol.* **2020**, *43*, 1674–1689. [CrossRef]
16. Yu, J.; Smith, J.D. Validation and application of a kinetic model for biomass gasification simulation and optimization in updraft gasifiers. *Chem. Eng. Process.-Process. Intensif.* **2018**, *125*, 214–226. [CrossRef]
17. Basu, P. *Biomass Gasification, Pyrolysis and Torrefaction*, 3rd ed.; Academic Press: London, UK, 2018.
18. Huang, F.; Jin, S. Investigation of biomass (pine wood) gasification: Experiments and Aspen Plus simulation. *Energy Sci. Eng.* **2019**, *7*, 1178–1187. [CrossRef]
19. Zhao, Z.; Jiang, J.; Wang, F. An economic analysis of twenty light olefin production pathways. *J. Energy Chem.* **2021**, *56*, 193–202. [CrossRef]
20. González-Vázquez, M.P.; Rubiera, F.; Pevida, C.; Pio, D.T.; Tarelho, L.A. Thermodynamic analysis of biomass gasification using aspen plus: Comparison of stoichiometric and non-stoichiometric models. *Energies* **2021**, *14*, 189. [CrossRef]
21. Wu, W.; Kawamoto, K.; Kuramochi, H. Hydrogen-rich synthesis gas production from waste wood via gasification and reforming technology for fuel cell application. *J. Mater. Cycles Waste Manag.* **2006**, *8*, 70–77. [CrossRef]
22. Pfeifer, C.; Koppatz, S.; Hofbauer, H. Steam gasification of various feedstocks at a dual fluidised bed gasifier: Impacts of operation conditions and bed materials. *Biomass Convers. Biorefinery* **2011**, *1*, 39–53. [CrossRef]
23. Anniwaer, A.; Chaihad, N.; Zahra, A.C.A.; Yu, T.; Kasai, Y.; Kongparakul, S.; Samart, C.; Abudula, A.; Guan, G. Steam co-gasification of Japanese cedarwood and its commercial biochar for hydrogen-rich gas production. *Int. J. Hydrogen Energy* **2021**, *46*, 34587–34598. [CrossRef]
24. Aljbour, S.H.; Kawamoto, K. Bench-scale gasification of cedar wood—Part I: Effect of operational conditions on product gas characteristics. *Chemosphere* **2013**, *90*, 1495–1500. [CrossRef]
25. Sun, Y.; Zhang, Z.; Seetharaman, S.; Liu, L.; Wang, X. Characteristics of low temperature biomass gasification and syngas release behavior using hot slag. *RSC Adv.* **2014**, *4*, 62105–62114. [CrossRef]
26. Kaushal, P.; Tyagi, R. Advanced simulation of biomass gasification in a fluidized bed reactor using ASPEN PLUS. *Renew. Energy* **2017**, *101*, 629–636. [CrossRef]
27. Sharma, A.K. Equilibrium modeling of global reduction reactions for a downdraft (biomass) gasifier. *Energy Convers. Manag.* **2008**, *49*, 832–842. [CrossRef]
28. Goswami, L.; Tejas Namboodiri, M.; Vinoth Kumar, R.; Pakshirajan, K.; Pugazhenthi, G. Biodiesel production potential of oleaginous Rhodococcus opacus grown on biomass gasification wastewater. *Renew. Energy* **2017**, *105*, 400–406. [CrossRef]
29. Hantoko, D.; Yan, M.; Prabowo, B.; Susanto, H.; Li, X.; Chen, C. Chapter 13—Aspen Plus Modeling Approach in Solid Waste Gasification. In *Current Developments in Biotechnology and Bioengineering*; Kumar, S., Kumar, R., Pandey, A., Eds.; Elsevier: Amsterdam, The Netherlands, 2019; pp. 259–281. [CrossRef]
30. Schneider, C.; Rincón Prat, S.; Kolb, T. Determination of active sites during gasification of biomass char with CO_2 using temperature-programmed desorption. Part 1: Methodology and desorption spectra. *Fuel* **2020**, *267*, 116726. [CrossRef]
31. Larkin, J.; Macken, N.; Schaffer, M.; Elkasabi, Y.; Mullen, C.A.; Boateng, A.A.; Bjornebo, L.; Spatari, S. A process simulation of guayule biorefining, including an exergy analysis. In *Energy Sustainability*; American Society of Mechanical Engineers: New York, NY, USA, 2016; Volume 50220, p. V001T13A001. [CrossRef]
32. Lee, J.C.; Lee, H.H.; Joo, Y.J.; Lee, C.H.; Oh, M. Process simulation and thermodynamic analysis of an IGCC (integrated gasification combined cycle) plant with an entrained coal gasifier. *Energy* **2014**, *64*, 58–68. [CrossRef]
33. Han, J.; Liang, Y.; Hu, J.; Qin, L.; Street, J.; Lu, Y.; Yu, F. Modeling downdraft biomass gasification process by restricting chemical reaction equilibrium with Aspen Plus. *Energy Convers. Manag.* **2017**, *153*, 641–648. [CrossRef]
34. Umeki, K.; Yamamoto, K.; Namioka, T.; Yoshikawa, K. High temperature steam-only gasification of woody biomass. *Appl. Energy* **2010**, *87*, 791–798. [CrossRef]
35. Kawamoto, K.; Wu, W.; Kuramochi, H. Development of Gasification and Reforming Technology using Catalyst at Lower Temperature for Effective Energy Recovery: Hydrogen Recovery Using Waste Wood. *J. Environ. Eng.* **2009**, *4*, 409–421. [CrossRef]
36. Yu, S.; Park, J.J.; Kim, M.; Ryu, C.; Park, J.J. Characterization of biochar and byproducts from slow pyrolysis of hinoki cypress. *Bioresour. Technol. Rep.* **2019**, *6*, 217–222. [CrossRef]
37. Viana, H.F.d.S.; Rodrigues, A.M.; Godina, R.; Matias, J.C.d.O.; Nunes, L.J.R. Evaluation of the physical, chemical and thermal properties of Portuguese maritime pine biomass. *Sustainability* **2018**, *10*, 2877. [CrossRef]
38. Eisermann, W.; Johnson, P.; Conger, W.L. Estimating thermodynamic properties of coal, char, tar and ash. *Fuel Process. Technol.* **1980**, *3*, 39–53. [CrossRef]

39. Shrivastava, P.; Kumar, A.; Tekasakul, P.; Lam, S.S.; Palamanit, A. Comparative investigation of yield and quality of bio-oil and biochar from pyrolysis of woody and non-woody biomasses. *Energies* **2021**, *14*, 1092. [CrossRef]
40. Popescu, F.; Mahu, R.; Ion, V.I.; Rusu, E. A Mathematical Model of Biomass Combustion Physical and Chemical Processes. *Energies* **2020**, *13*, 6232. [CrossRef]
41. Minami, E.; Saka, S. Biomass resources present in Japan—Annual quantities grown, unused and wasted. *Biomass Bioenergy* **2005**, *29*, 310–320. [CrossRef]
42. Chmielniak, T.; Stepien, L.; Sciazko, M.; Nowak, W. Effect of pyrolysis reactions on coal and biomass gasification process. *Energies* **2021**, *14*, 5091. [CrossRef]
43. Nikoo, M.B.; Mahinpey, N. Simulation of biomass gasification in fluidized bed reactor using ASPEN PLUS. *Biomass Bioenergy* **2008**, *32*, 1245–1254. [CrossRef]
44. Kato, Y.; Enomoto, R.; Akazawa, M.; Kojima, Y. Characterization of Japanese cedar bio-oil produced using a bench-scale auger pyrolyzer. *SpringerPlus* **2016**, *5*, 177 . [CrossRef]
45. Mendes, D.; Mendes, A.; Madeira, L.M.; Iulianelli, A.; Sousa1, J.M.; Basile, A. The water-gas shift reaction: from conventional catalytic systems to Pd-based membrane reactors—A review. *Asia-Pac. J. Chem. Eng.* **2010**, *5*, 111–137. [CrossRef]
46. Umeki, K.; Son, Y.I.; Namioka, T.; Yoshikawa, K. Basic Study on Hydrogen-rich Gas Production by High Temperature Steam Gasification of Solid Wastes. *J. Environ. Eng.* **2009**, *4*, 321–327. [CrossRef]
47. Prasertcharoensuk, P.; Bull, S.J.; Phan, A.N. Gasification of waste biomass for hydrogen production: Effects of pyrolysis parameters. *Renew. Energy* **2019**, *143*, 112–120. [CrossRef]
48. Squara, P.; Scheeren, T.W.; Aya, H.D.; Bakker, J.; Cecconi, M.; Einav, S.; Malbrain, M.L.; Monnet, X.; Reuter, D.A.; van der Horst, I.C.; et al. Metrology part 1: Definition of quality criteria. *J. Clin. Monit. Comput.* **2021**, *35*, 17–25. [CrossRef]
49. Zeng, Y.; He, H.; Qin, K.; Zhang, M.; An, Z.; Huang, H. Practical application of the sigma-metric run size nomogram for multistage bracketed statistical quality control analysis of eight enzymes. *Clin. Chim. Acta* **2019**, *492*, 57–61. [CrossRef] [PubMed]
50. Honma, S.; Hata, T.; Watanabe, T. Effect of catalytic pyrolysis conditions using pulse current heating method on pyrolysis products of wood biomass. *Sci. World J.* **2014**, *2014*, 720527 . [CrossRef]
51. Morin, M.; Pécate, S.; Hémati, M. Experimental study and modelling of the kinetic of biomass char gasification in a fluidized bed reactor. *Chem. Eng. Res. Des.* **2018**, *131*, 488–505. [CrossRef]